Functional role of internal water molecules in rhodopsin revealed by x-ray crystallography

Tetsuji Okada*†‡§, Yoshinori Fujiyoshi*‡, Maria Silow¶, Javier Navarro¶, Ehud M. Landau¶, and Yoshinori Shichida*†

*Department of Biophysics, Graduate School of Science, Kyoto University, and †Core Research for Evolution Science and Technology (CREST), Japan Science and Technology Corporation, Kyoto 606-8502, Japan; ‡Biological Information Research Center, National Institute of Advanced Industrial Science and Technology, Tokyo 135-0064, Japan; and ¶Membrane Protein Laboratory, Department of Physiology and Biophysics, and Sealy Centers for Structural Biology and Molecular Science, University of Texas Medical Branch, Galveston, TX 77555-0437

Edited by Jeremy Nathans, Johns Hopkins University School of Medicine, Baltimore, MD, and approved February 26, 2002 (received for review December 12, 2001)

Activation of G protein-coupled receptors (GPCRs) is triggered and regulated by structural rearrangement of the transmembrane heptahelical bundle containing a number of highly conserved residues. In rhodopsin, a prototypical GPCR, the helical bundle accommodates an intrinsic inverse-agonist 11-*cis*-retinal, which undergoes photo-isomerization to the *all-trans* form upon light absorption. Such a trigger by the chromophore corresponds to binding of a diffusible ligand to other GPCRs. Here we have explored the functional role of water molecules in the transmembrane region of bovine rhodopsin by using x-ray diffraction to 2.6 Å. The structural model suggests that water molecules, which were observed in the vicinity of highly conserved residues and in the retinal pocket, regulate the activity of rhodopsin-like GPCRs and spectral tuning in visual pigments, respectively. To confirm the physiological relevance of the structural findings, we conducted single-crystal microspectrophotometry on rhodopsin packed in our three-dimensional crystals and show that its spectroscopic properties are similar to those previously found by using bovine rhodopsin in suspension or membrane environment.

Cell surface membrane receptors mediate a variety of biological signaling processes that are triggered by a multitude of diffusible molecules or light in the case of visual pigments. G protein-coupled receptors (GPCRs), including the rhodopsin-like family as a dominant subgroup, are the largest group of membrane receptors. Many of the members are considered as primary drug targets for various medical and pharmacological interventions. These receptors appear to be activated by a mechanism involving common heptahelical transmembrane architecture that undergoes major rearrangement upon signal reception, resulting in activation of the heterotrimeric G protein molecules.

Rhodopsin from retinal rod cells mediates scotopic vision. It is a unique member among GPCRs in that it contains an intrinsic inverse-agonist, the 11-*cis*-retinal. Photon absorption results in retinal isomerization to the *all-trans* configuration, which drives the protein to the active metarhodopsin form (M II) (1). Visual pigments mediating color vision in cone cells share a common mechanism to evoke a cellular signaling cascade (2) through interaction between the M II state and the G protein. A view of the seven helices of bovine rhodopsin was provided by electron crystallography in 1993 (3), and an x-ray crystallographic study recently determined its structure at 2.8-Å resolution (4). This structure provided the template model at high resolution for the rhodopsin-like GPCRs and has been further refined at the same resolution (5).

The 11-*cis*-retinal chromophore is covalently bound to Lys-296 in transmembrane helix VII by a protonated Schiff base linkage, which is stabilized by the negatively charged counterion Glu-113 in helix III. Disruption of this salt bridge (6) upon proton transfer is thought to trigger conformational changes in rhodopsin (7), which are necessary for G protein activation. This neutralization process corresponds to binding of a cationic part in a diffusible ligand to other rhodopsin-like receptors (8) and is one of the critical determinants of activity. Therefore, the nature of the Schiff base–counterion interaction in the ground state of rhodopsin has been a focus of many previous studies (9–12).

Previous NMR and Fourier transform IR studies predicted that the interaction between the Schiff base and the counterion would be mediated by water molecules (11–13). The crystal structure, however, revealed that the side chain of Glu-113 is located in the vicinity of the Schiff base nitrogen, suggesting a direct contact between them. Moreover, the crystal structure revealed unexpectedly that the second extracellular loop connecting transmembrane helices IV and V formed a part of the chromophore-binding site. This implies that some charged and/or polar residues in this loop, which were not previously taken into account, affect the electrostatic environment of the chromophore, including the protonated Schiff base. These findings present new challenges for understanding the molecular mechanism of rhodopsin activation as well as color tuning in cone visual pigments.

Furthermore, activity and ligand binding of rhodopsin and other GPCRs are significantly affected by mutations in the cytoplasmic half of the transmembrane region, which contains many of the highly conserved residues. In some GPCRs, sensitivity to cations such as sodium ion was demonstrated to involve a part of the interhelical region (14–16). Detailed structural information on the transmembrane region is needed to elucidate the exact molecular mechanism underlying these observations. Here we have refined the structural model of bovine rhodopsin by using x-ray diffraction to 2.6 Å, thereby providing a more detailed view of the transmembrane region where several water molecules are found to play critical roles. We also show by microspectrophotometry that rhodopsin molecules in three-dimensional (3D) crystals undergo a series of transitions from the ground state to the photoreaction intermediates, indicating functional similarity of rhodopsin in the crystal lattice to that in the native environment.

Methods

Crystallographic Refinement. Purification and crystallization of rhodopsin from bovine rod outer segment membranes were carried out as described (17). The crystals were first soaked in a mercury solution that significantly improves diffraction power and then in a cryo-solution and flash frozen in liquid nitrogen (4). X-ray diffraction data sets were collected at 100 K by using

This paper was submitted directly (Track II) to the PNAS office.

Abbreviations: GPCRs, G protein-coupled receptors; M II, active form of rhodopsin; 3D, three-dimensional.

Data deposition: The atomic coordinates have been deposited in the Protein Data Bank, www.rcsb.org (PDB ID code 1L9H).

§To whom reprint requests should be addressed. E-mail: okada@photo2.biophys.kyoto-u.ac.jp.

The publication costs of this article were defrayed in part by page charge payment. This article must therefore be hereby marked "*advertisement*" in accordance with 18 U.S.C. §1734 solely to indicate this fact.

a MAR165 charge-coupled device detector in beamline BL41XU at SPring-8 (Hyogo, Japan) in dim red light environment to prevent photoreaction of rhodopsin. The data sets were indexed, integrated, and scaled with HKL2000 (32). Both CNS (33) and DETWIN in the CCP4 package (34) were used to estimate twin fractions in the data sets. The starting model for refinement was constructed by using two structures (Protein Data Bank ID codes 1F88 and 1HZX) in part and placed in the lattice of a new data set by AMORE (35). After rigid body refinement, conjugate gradient energy minimization under NCS restraints, σA-weighted $2F_o - F_c$ and $F_o - F_c$ maps were calculated in CNS by using undetwinned data as described previously (5). XFIT (36) was used for manual modification of the model, including allocation of water molecules. The final round of energy minimization and individual B factor refinement for each data set was run without NCS restraints. The coordinates from data set 1 in Table 2 have been deposited with the Protein Data Bank, ID code 1L9H.

Single-Crystal Microspectrophotometry. Visible absorption spectra from a 3D crystal were recorded by using a microspectrophotometer similar to that used previously with crystals of bacteriorhodopsin (37). In brief, a crystal placed in a nylon loop was mounted on a goniometer head that was settled on a microspectrophotometer. Probe light was introduced through a fiber cable with a diameter of 50 μm from a xenon lamp except for the spectrum in Fig. 3*c,* for which a D_2 lamp was used to cover the near-UV wavelength region. Photoreaction of a crystal was triggered by exposure to light from a tunable argon laser (Melles Griot, Irvine, CA). The diameter of the laser light (0.8 mm) was large enough to cover a rod-shaped crystal with a maximum dimension of ≈0.5 mm.

Results and Discussion

Crystallographic Refinement. 3D crystals of bovine rhodopsin were obtained by the hanging-drop vapor diffusion method with high gradient concentration as described before (17). They were rather poor in terms of isomorphism and contained various amounts of twin fractions ranging from 0.1 to 0.4. In the current refinement we therefore treated three data sets independently to confirm reproducibility of the new features. The statistics are summarized in Table 1. Two of the data sets (2 and 3), although limited to 2.7 Å, have twice the redundancy of the previous data set. A structural model of bovine rhodopsin to 2.6-Å resolution refined by using data set 1 is representative of the three new sets of coordinates and is described below. The asymmetric unit contains two rhodopsin molecules, denoted as A and B in the following, the former being a better-refined model. Some of the electron densities at the dimer interface, assigned previously to nonyl glucoside and heptanetriol (5), are found to be connected to each other. We fitted these densities by two hydrocarbon chains because it is likely that our crystals contain some native lipids (17). The rms deviations of the current model from 1HZX (5) are 0.42 Å and 0.60 Å for the 2,556 main-chain and 2,488 side-chain atoms, respectively. The configuration of retinal in the present structure at 2.6 Å is much closer to that in 1F88 around C13–C15, and to that in 1HZX around C9.

The initial structural model of bovine rhodopsin contained only one water molecule in the transmembrane region (4), which was hydrogen bonded to Asp-83 and Gly-120 in molecule A (Table 2). Although further refinement using the same data set assigned additional sites (5), this study did not unambiguously reveal the functional role of water in the transmembrane region of rhodopsin. Because only one data set was available and the results of two previous studies were not consistent, identification of water molecules remained unclear at that time. Therefore we have collected numerous data sets with reflections exceeding the previous limit (2.8 Å). A detailed examination of the resulting electron density map has consistently confirmed all of the water molecules suggested previously in both molecule A and molecule B. Using the current data sets, we could allocate more water molecules in the transmembrane region of both A and B. The primary aim of this study, to unequivocally present hydrogen-bonded water molecules in the transmembrane region of bovine rhodopsin, in particular around the retinal-binding site, which is crucial for understanding receptor function, is thereby accomplished.

Table 1. X-ray data and refinement statistics

	Value		
Measurement	Data set 1	Data set 2	Data set 3
Data statistics			
Resolution, Å	2.6	2.7	2.7
Unit cell			
a, Å	96.75	97.58	97.79
b, Å	96.75	97.58	97.79
c, Å	149.3	149.4	149.5
Twin fraction	0.20	0.30	0.29
Mosaicity, °	0.63	0.65	0.32
Total observations	124,947	232,484	225,843
Unique observations	36,092	34,579	33,198
R_{merge}, % (outer shell)	9.90 (55.5)	14.8 (65.0)	15.3 (71.4)
Completeness, % (outer shell)	85.6 (40.0)	90.2 (47.4)	86.2 (36.7)
$I/\sigma(I)$ (outer shell)	12.0 (1.0)	11.0 (0.94)	11.0 (1.9)
Wilson B factor, Å^2	69.4	66.1	59.6
Refinement statistics			
R_{cryst}, %	18.8	17.9	17.5
R_{free}, %	22.5	21.2	22.2
rms deviation of bonds			
Length, Å	0.013	0.012	0.013
Angles, °	1.52	1.50	1.50
Average B factors, Å^2	69.1	62.0	57.5

Data set 1 was collected with an exposure time of 30 sec per 1.0° oscillation for the total of 90°. Data sets 2 and 3 were collected with exposure time of 10 sec per 1.5° oscillation for the total of 180°. The crystal-to-detector distance and x-ray wavelength were 190 mm and 1.000 Å, respectively, for all the data sets. $R_{merge} = \Sigma_{hkl} \Sigma_i | I_i(hkl) - \langle I(hkl) \rangle | / \Sigma_{hkl} \Sigma_i I_i(hkl)$. $R_{cryst} = \Sigma_{hkl} | F_o - F_c | / \Sigma_{hkl} | F_o |$. R_{free} data were calculated from a set of 5% randomly selected reflections that were omitted from refinement.

Water Molecules in the Transmembrane Region. Seven water molecules are consistently found in both molecule A and molecule B (Fig. 1*a*) when the current data sets are used. Many of the highly conserved residues among rhodopsin-like GPCRs are found to form binding sites for these water molecules, including Asn-73 (2.40, numbering according to ref. 18), Asp-83 (2.50), Cys-264 (6.47), Asn-302 (7.49), and Tyr-306 (7.53) (Table 2). In addition, other residues participating in the water-binding sites are particularly conserved in a variety of visual pigments, regardless of the distance from the chromophore-binding site.

Water molecules 1a, 1b, and 1c are clustered in the region where the previous structure contained only one water molecule in molecule A (4). This water cluster is linked to Asn-302, a key residue which is at the initial position of the so-called NPXXY motif commonly found in the helix VII of the rhodopsin-like GPCRs (Table 2). The water cluster mediates the interaction of the side chain of Asn-302 with residues in helices II, III, VI, and VII by means of a hydrogen-bonded network, resulting in inter-helical constraints (Fig. 1*b*). Disruption of these constraints is likely to be involved in the activation process (19, 20). In particular, the side chain of Asp-83 in helix II, a highly conserved residue among the rhodopsin-like GPCRs, also participates in this hydrogen-bonded network. A structural link between Asp-83 and Tyr-301 in helix VII by a water molecule is also

BIOPHYSICS

Table 2. Comparison of the water-binding sites among the three sets of coordinates of rhodopsin

Site no.	Residues for hydrogen bonds	1F88		1HZX		Current work	
		A*	B*	A*	B*	A* (*B*, Å^2)†	B* (*B*, Å^2)†
1a	D83, G120	971	—	—	2009	2015 (41)	2009 (38)
1b	D83, S298, N302	—	—	—	—	2017 (50)	2016 (48)
1c	M257, Y301, N302	—	—	—	2008	2020 (34)	2008 (35)
2a	E181, S186, C187	—	—	2014	—	2014 (43)	2018 (49)
2b	F91, E113	—	—	—	—	2021 (53)	2022 (49)
3	C264, Y268, P291	—	—	Zn964	—	964 (35)	2019 (63)
4	T62, N73, Y306	—	—	—	—	2024 (34)	2025 (52)

*The identifiers for the water molecules are residue numbers in the individual PDB file.
†Temperature factor, *B*, of each site is shown (in parentheses) from the coordinate refined against data set 1 in Table 1.

consistent with our recent Fourier transform IR study on the Y301F mutant (T. Oura, A. Terakita, H. Kandori, and Y.S., unpublished observation). Asp-83 is directly hydrogen-bonded to Asn-55 (1.50) in helix I, and these two are frequently referred to as the N–D pair in rhodopsin-like GPCRs. Thus, three highly conserved residues, Asn-55, Asp-83, and Asn-302, constitute a hydrogen-bonded chain in the ground state structure of bovine rhodopsin. Other residues in this region, Gly-120, Met-257, Ser-298, and Tyr-301, appear to constrain the rhodopsin structure, stabilizing the ground state and resulting in lower activity than other rhodopsin-like GPCRs. The importance of this region was clearly demonstrated by results indicating that the cytoplasmic side in bovine rhodopsin becomes exposed upon activation, allowing an Ab to bind residues from Val-304 to Lys-311 (21).

The space occupied by the water molecules overlaps with a putative sodium-binding site proposed for other members in rhodopsin-like GPCRs (14–16). In some GPCRs, sodium participates in the regulatory mechanism for both activity and ligand binding. We note that a hydroxyl-bearing amino acid (Ser or Thr) at the position corresponding to Ala-124 (3.39, as numbered in ref. 18) in bovine rhodopsin is commonly found in rhodopsin-like GPCRs other than visual pigments (Fig. 1*b*). Our current model suggests that a hydroxyl side chain at this position would contribute to the sodium-binding site, consistent with a recent study on dopamine D_2 receptor (16). Another residue that might possibly be involved in the Wat1 site is a highly conserved Asp-6.44 (Phe-261 in bovine rhodopsin) in the subfamily of glycoprotein hormone receptors such as thyroid-stimulating hormone receptor, as disruption of the interaction between Asp-6.44 and Asn-7.49 (Asn-302 in bovine rhodopsin) was shown to evoke constitutive activity (22). Assuming minimal deviation of the backbone structure between those receptors and rhodopsin, Wat1c is favorably located to bridge these two side chains.

Presence of an ion and/or polar side chains at the Wat1 site in the general class of GPCRs does not exclude possible involvement of water molecules, which could be associated with the ion. Our findings argue that the architecture of the hydrogen-bonding network among helices II, III, VI, and VII may vary for distinct classes of receptors. This network probably involves the interhelical residue positions described above and is modulated upon binding of ions and water. The presence of the water cluster in the rhodopsin structure strongly suggests flexible regulation of activity by hydrogen-bond patterning at this site in GPCRs. Such electrostatic shuffling would partly explain substates of GPCRs exhibiting distinct affinity for a ligand and a target G protein.

Hydrogen-Bonded Network Around the Retinal. The second site containing two water molecules (Wat2a and -2b) includes the retinal Schiff base. Presence of Wat2a was suggested only in molecule A by the previous refinement (5). With the current data sets and a model structure calculated before the inclusion of water molecules, two strong positive difference electron densities appeared around the Schiff base in both molecule A and molecule B (Fig. 2*a*). Wat2a is located between the side chains of Glu-181 and Ser-186, consistent with the previous work, and Wat2b appears in the vicinity of Glu-113, the counterion of the protonated Schiff base. Wat2a is also possibly linked to the side chain of Glu-113 via peptide amide of Cys-187 (Fig. 2*b*). Wat2b does not reside between the Schiff base and the carboxyl group of Glu-113 as expected before, but likely stabilizes this salt bridge by lowering the pK_a of Glu-113. Wat2b fills a small but prominent spatial gap between helices II and III at the retinal-binding pocket. Although it appears that our current model still needs to be reconciled with the concept of "complex counterion" proposed from NMR results (11, 12), experimental observations by Fourier transform IR of water signals around the Schiff base can be explained well (13). Our model is also consistent with a previous study of the E113D rhodopsin mutant, which showed that the shorter side chain of aspartate could function as the counterion, resulting in a slightly red-shifted absorption (23), whereas the NMR studies predicted a distance between the counterion and the Schiff base too large to explain the results of this mutation.

The position of Wat2a is significant in terms of the mechanism of color regulation in the related retinal proteins, including cone visual pigments. In the long-wavelength cone visual pigments (green and red in human), a His residue at the position of Glu-181 in bovine rhodopsin has been demonstrated to bind a chloride ion, shifting the absorption maximum to the red (24). Presence of Wat2a in these chloride-binding pigments is suggested by our Fourier transform IR study on the chicken red pigment (25). Moreover, it was recently shown that the E181Q mutation of bovine rhodopsin caused a 10-nm shift of its absorption maximum compared with the wild type and that Glu-181 can act as a direct counterion of the protonated Schiff base in the squid retinal photoisomerase retinochrome (26). These items of evidence support the idea that rearrangement of the residues and water molecules in site 2 of our current model most likely plays a crucial role in the spectral tuning of the diverse family of eukaryotic retinal proteins. Glu-181 is located in the middle of a cluster of three polar residues, Tyr-191, Tyr-192, and Tyr-268, whose hydroxyl groups cover part of the retinal-binding pocket near C9. Thus we find a continuous hydrogen-bond network that lies in the extracellular side of the chromophore-binding site, covering a distance of >17 Å from the hydroxyl group of Tyr-192 to the peptide amide of Phe-91 (Fig. 2*b*). This observation of network implies that replacement of a single amino acid at a given position in this region can induce long-range effects on the spectral properties of visual pigments and emphasizes the importance of taking residue–residue interactions into account for elucidating the mechanism of color tuning. A recent molecular orbital calculation study is consistent with this notion (27). Additionally, an electrostatic link between the counterion and E181 by the peptide bond of Cys-187 and Wat2a might also explain some previous spectroscopic obser-

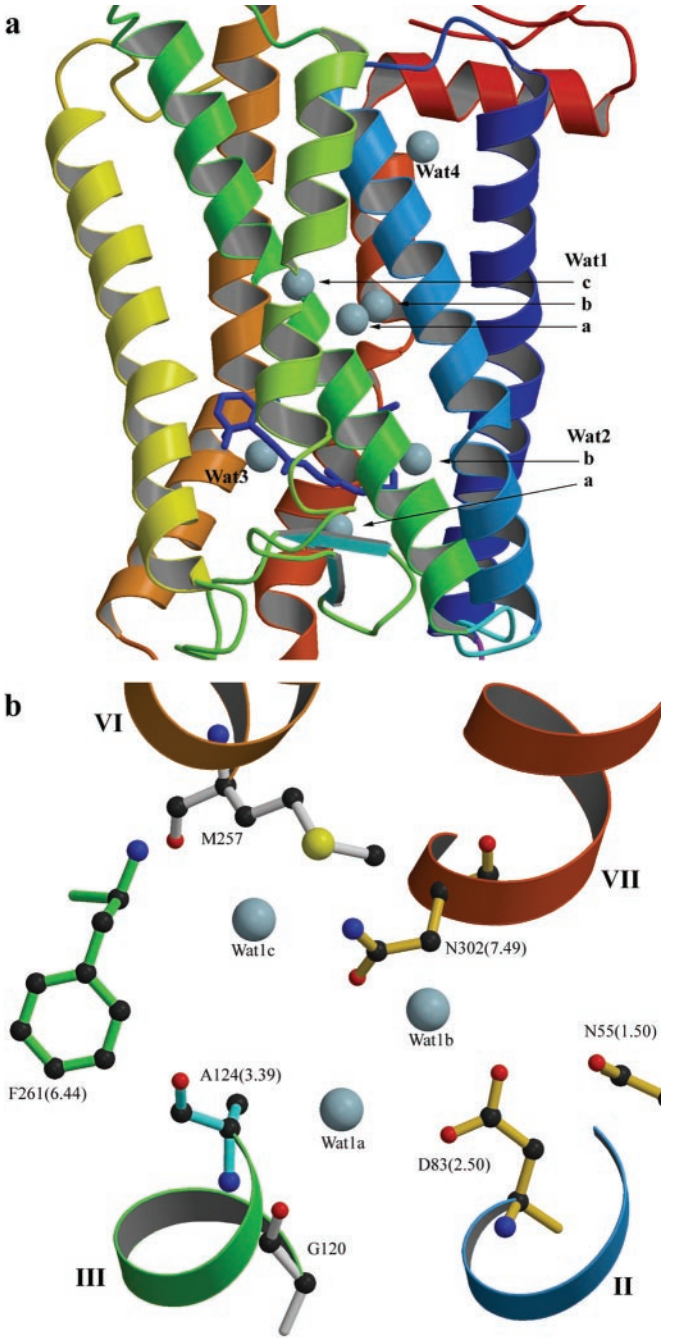

Fig. 1. (*a*) Global view of the transmembrane helical region of the refined bovine rhodopsin structure. The cytoplasmic surface is shown in the upper side. The four water-binding sites (Wat1–4) include seven water molecules (light blue spheres). Details of the sites are summarized in Table 2. (*b*) Detailed view of the Wat1 site. The residues surrounding Wat1a, -b, and -c are shown as ball-and-stick representation in standard atom colors. Colors of the stick are yellow for the conserved residues, cyan for Ala-124, and green for Phe-261. Numbers in parentheses are according to ref. 18. Figures were prepared with MOLSCRIPT (38) and RASTER3D (39).

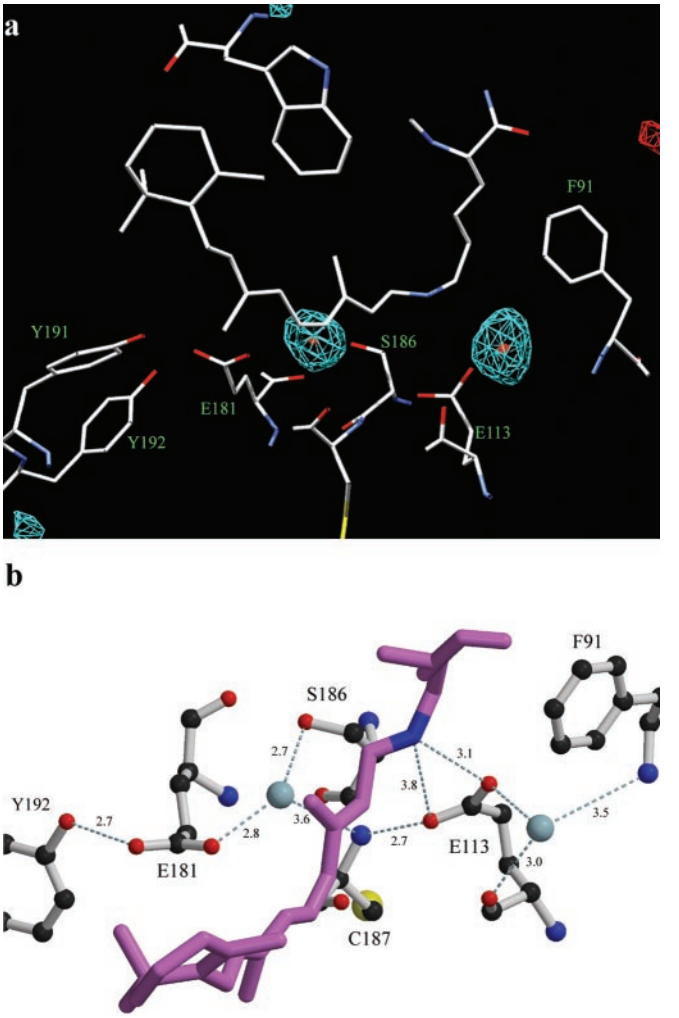

Fig. 2. (*a*) View of the retinal-binding site and electron densities for the two water molecules (Wat2a and Wat2b, red spheres) found in the vicinity of retinal Schiff base. σA-weighted $F_o - F_c$ omit map calculated for the waters at 2.6 Å is contoured at 4.0 σ with positive densities in blue. The figure was prepared with SPDBV (40). (*b*) Hydrogen bond network around the Schiff base. Retinal and Lys-296 are shown in purple with the NZ position in blue, and the surrounding residues are represented as ball-and-stick figures in standard colors. Wat2a and Wat2b are shown as light-blue spheres. Each of the distances (Å) is an averaged value from molecule A and molecule B in an asymmetric unit. The figure was prepared with MOLSCRIPT (38) and RASTER3D (39).

vations on mutational effects of Glu-113 on perturbation of the chromophore around C12 (28).

Other Water Molecules. Wat3 was previously assigned as a zinc ion only in molecule A with 50% occupancy, but no specific ligand could be found around it (5). In the present analysis, we fitted the corresponding electron density with water having reasonable temperature factors for both molecule A and molecule B. This water is surrounded by the peptide main chains of helices VI and VII. Among the residues forming the binding site, Cys-264 and Pro-267 are highly conserved in the rhodopsin-like GPCRs. Because this region in helix VI is highly bent, its functional role in activation has been suggested. Thus it is possible that electrostatic interaction between helices VI and VII through Wat3 might stabilize the ground state of rhodopsin.

Wat4 mediates interaction between helices I and II at the cytoplasmic surface. The residues forming the binding site include Thr-62 and Asn-73. The former is highly conserved as either threonine or serine in the visual pigments of vertebrates but not of invertebrates, whereas the latter is commonly observed in the rhodopsin-like GPCRs. Therefore this region might be critical for activation and/or G protein specificity.

Single-Crystal Microspectrophotometry. To confirm the physiological relevance of the findings described above, we examined by

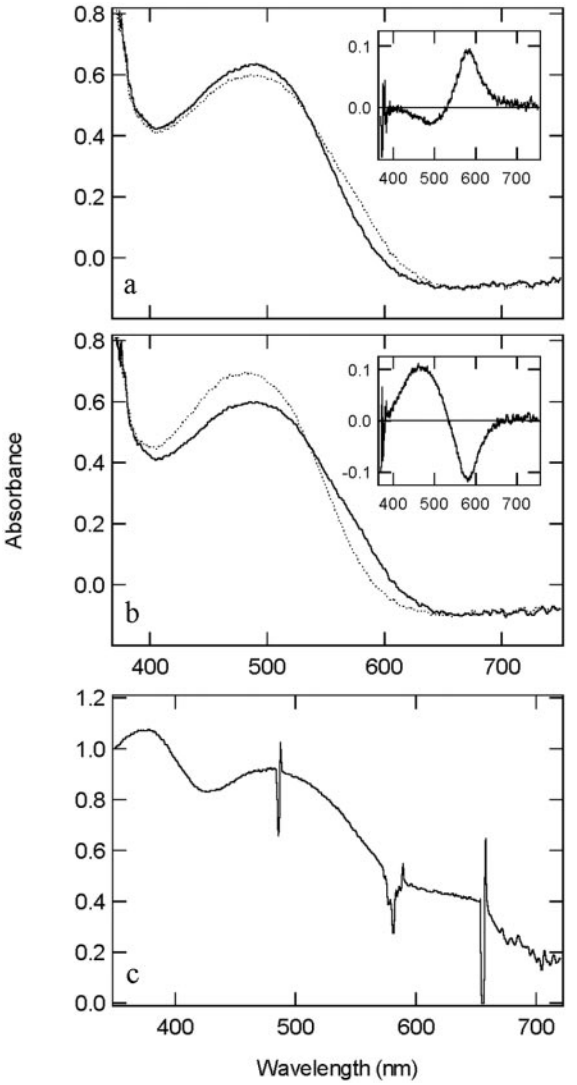

Fig. 3. Rhodopsin absorption spectra obtained by single-crystal microspectrophotometry. (*a*) Ground state spectrum of a rhodopsin crystal (solid line). After illumination with argon laser (488 nm, 7 mW) at 100 K for 1 min, the spectrum shown by the dotted line was recovered. (*Inset*) The difference spectrum between the dotted and solid curves, which is consistent with formation of bathorhodopsin (29). (*b*) The illuminated crystal (solid line, identical to the dotted line in spectrum *a*) was warmed up to 140 K (rate = 3 K/min) and cooled down to 100 K. The spectrum shown in the dotted line was recovered. The interval between the onset of warming and the measurement at 100 K was ≈15 min. (*Inset*) The difference spectrum between the two curves, which is consistent with the spectral change from bathorhodopsin to lumirhodopsin. (*c*) The rhodopsin crystal was first illuminated at 5°C for 3 min with >540-nm light and flash frozen with liquid nitrogen. The time interval between the end of illumination and freezing was ≈3 min. The 380-nm product corresponds to M II. Spikes in the spectrum are due to fluctuation of the probe light from the D_2 lamp.

single-crystal microspectrophotometry whether rhodopsin packed in our 3D crystals exhibits spectroscopic properties similar to those previously found for bovine rhodopsin in suspension or membrane environment (Fig. 3). The absorption maximum of rhodopsin in the crystal was ≈495 nm at 100 K (Fig. 3*a*), similar to that of a hydrated rhodopsin–phosphatidylcholine film measured at 77 K (13). In our rod-shaped crystals, some fraction of the chromophore's dipole moment is perpendicular to the plane of the cryoloop, which limits the maximal amount of the excitable rhodopsin molecules in the crystal in the following experiments.

Photoreaction intermediates of bovine rhodopsin have been well established by low-temperature spectroscopic studies (29). These include the batho, lumi, M I, and M II states that are successively observed after illumination and upon warming up from liquid nitrogen temperature to room temperature and also have been confirmed by flash photolysis at room temperature (30). In this study, a 3D crystal of bovine rhodopsin was illuminated with blue light at 100 K. Compared to its absorption spectrum in the ground state, the spectrum of the crystal shifted to longer wavelength with an intersection point of ≈530 nm and a maximum in the difference spectrum at ≈580 nm (Fig. 3*a*), which is consistent with formation of bathorhodopsin (29). When the illuminated rhodopsin crystal was warmed up to 140 K, both depletion at approximately 570 nm and increase at approximately 460 nm were observed. The difference spectrum characterizing this process (Fig. 3*b*) is consistent with the spectral change from bathorhodopsin to lumirhodopsin (29).

To detect the later metaintermediates (M I and M II), we first illuminated the crystals at 5°C and then flash froze them within a few minutes. As crystals of bovine rhodopsin are readily degraded upon exposure to visible light at 5°C (17), we have used several solvent conditions to stabilize the crystals, thereby allowing us to detect the late intermediates. It is also likely that the degree of mercury binding affects retention of the crystal lattice (T.O., unpublished observation). Depending on the illumination time and the interval between the end of illumination and freezing, we detected formation of different amounts of the blue-shifted photoproduct with an absorption maximum of ≈380 nm. An example is shown in Fig. 3*c*. Considering the lifetime of the intermediates of rhodopsin at 5°C (31), it is likely that the 380-nm product corresponds to M II. In conclusion, our spectroscopy data indicate that the photoreaction of rhodopsin packed in 3D crystals is consistent with that of rhodopsin observed previously in either membrane or solution environment.

Conclusions

Our current model offers further insights into the molecular mechanism for the functionally important salt bridge stabilization, as well as color regulation in the visual pigment and the related retinal proteins. We further show that many of the highly conserved residues among rhodopsin-like GPCRs are found to be associated with water molecules that appear to mediate intramolecular interaction and offer a regulatory mechanism of activity. Based on the refined model and the 3D crystals that are capable of forming M II-like photoproduct, further crystallographic studies should unveil the molecular mechanism of rhodopsin activation.

We are grateful to A. Royant for help with microspectrophotometry and valuable discussions, to M. Kawamoto for excellent conditioning of the beamline BL41XU at SPring-8, to C. A. Maxwell for expert experimental assistance, and to D. Bourgeois for help with microspectrophotometry. M.S. acknowledges the Swedish Foundation for International Cooperation in Research and Higher Education (STINT) for a postdoctoral fellowship. This work was supported by grants from the Japan Society for Promotion of Science, Japan Biological Informatics Consortium (JBIC) and the Robert A. Welch Foundation. Support of the Howard Hughes Medical Institute to the Membrane Protein Laboratory at the Univ. of Texas Medical Branch is greatly appreciated.

1. Hofmann, K. P. (2000) in *Handbook of Biological Physics*: *Molecular Mechanisms in Visual Transduction*, eds. Stavenga, D. G., Degrip, W. J. & Pugh, E. N., Jr. (Elsevier/North–Holland, New York), Vol. 3, pp. 91–142.
2. Yoshizawa, T. (1992) *Photochem. Photobiol.* **56,** 859–867.
3. Schertler, G. F., Villa, C. & Henderson, R. (1993) *Nature (London)* **362,** 770–772.
4. Palczewski, K., Kumasaka, T., Hori, T., Behnke, C. A., Motoshima, H., Fox, B. A., Le Trong, I., Teller, D. C., Okada, T., Stenkamp, R. E., *et al.* (2000) *Science* **289,** 739–745.

5. Teller, D. C., Okada, T., Behnke, C. A., Palczewski, K. & Stenkamp, R. A. (2001) *Biochemistry* **40,** 7761–7772.
6. Robinson, P. R., Cohen, G. B., Zhukovsky, E. A. & Oprian, D. D. (1992) *Neuron* **9,** 719–725.
7. Farren, D. L., Altenbach, C., Yang, K., Hubbell, W. L. & Khorana, H. G. (1996) *Science* **274,** 768–770.
8. Strader, C. D., Sigal, I. S., Candelore, M. R., Rands, E., Hill, W. S. & Dixon, R. A. (1988) *J. Biol. Chem.* **263,** 10267–10271.
9. Honig, B., Dinur, U., Nakanishi, K., Balogh-Nair, V., Gawinowics, M. A., Arnaboldi, M. & Motto, M. G. (1979) *J. Am. Chem. Soc.* **101,** 7084–7086.
10. Ebrey, T. G. (2000) *Methods Enzymol.* **315,** 196–207.
11. Verhoeven, M. A., Creemers, A. F. L., Bovee-Geurts, P. H. M., Degrip, W. J., Lugtenburg, J. & De Groot, H. J. M. (2001) *Biochemistry* **40,** 3282–3288.
12. Eilers, M., Reeves, P. J., Ying, W., Khorana, H. G. & Smith, S. O. (1999) *Proc. Natl. Acad. Sci. USA* **96,** 487–492.
13. Nagata, T., Terakita, A., Kandori, H., Kojima, D., Shichida, Y. & Maeda, A. (1997) *Biochemistry* **36,** 6164–6170.
14. Horstman, D. A., Brandon, S., Wilson, A. L., Guyer, C. A., Cragoe, E. J. & Limbird, L. E. (1990) *J. Biol. Chem.* **265,** 21590–21595.
15. Martin, S., Botto, J. M., Vincent, J. P. & Mazella, J. (1999) *Mol. Pharmacol.* **55,** 210–215.
16. Neve, K. A., Cumbay, M. G., Thompson, K. R., Yang, R., Buck, D. C., Watts, V. J., DuRand, C. J. & Teeter, M. M. (2001) *Mol. Pharmacol.* **60,** 373–381.
17. Okada, T., Le Trong, S., Fox, B. A., Behnke, C. A., Stenkamp, R. E. & Palczewski, K. (2000) *J. Struct. Biol.* **130,** 73–80.
18. Ballesteros, J. A. & Weinstein, H. (1995) *Methods Neurosci.* **25,** 366–425.
19. Gether, U. & Kobilka, B. K. (1998) *J. Biol. Chem.* **273,** 17979–17982.
20. Sheikh, S. P., Zvyaga, T. A., Lichtarge, O., Sakmar, T. P. & Bourne, H. R. (1996) *Nature (London)* **383,** 347–350.
21. Abdulaev, N. G. & Ridge, K. D. (1998) *Proc. Natl. Acad. Sci. USA* **95,** 12854–12859.
22. Govaerts, C., Lefort, A., Costagliola, S., Wodak, S. J., Ballesteros, J. A., Van Sande, J., Pardo, L. & Vassart, G. (2001) *J. Biol. Chem.* **276,** 22991–22999.
23. Sakmar, T. P., Franke, R. R. & Khorana, H. G. (1989) *Proc. Natl. Acad. Sci. USA* **86,** 8309–8313.
24. Wang, Z., Asenjo, A. B. & Oprian, D. D. (1993) *Biochemistry* **32,** 2125–2130.
25. Hirano, T., Imai, H., Kandori, H. & Shichida, Y. (2001) *Biochemistry* **40,** 1385–1392.
26. Terakita, A., Yamashita, T. & Shichida, Y. (2000) *Proc. Natl. Acad. Sci. USA* **97,** 14263–14267.
27. Kusnetzow, A., Dukkipati, A., Babu, K. R., Singh, D., Vought, B. W., Knox, B. E. & Birge, R. R. (2001) *Biochemistry* **40,** 7832–7844.
28. Lin, S. W., Sakmar, T. P., Franke, R. R., Khorana, H. G. & Mathies, R. A. (1992) *Biochemistry* **31,** 5105–5111.
29. Yoshizawa, T. & Shichida, Y. (1982) *Methods Enzymol.* **81,** 333–354.
30. Lewis, J. W. & Kliger, D. S. (1992) *J. Bioenerg. Biomembr.* **24,** 201–210.
31. Kibelbek, J., Mitchell, D. C., Beaxh, J. M. & Litman, B. J. (1991) *Biochemistry* **30,** 6761–6788.
32. Otwinowski, Z. & Minor, W. (1997) *Methods Enzymol.* **276,** 307–326.
33. Brünger, A. T., Adams, P. D., Clore, G. M., DeLano, W. L., Gros, P., Grosse-Kunstleve, R. W., Jiang, J. S., Kuszewski, J., Nilges, M., Pannu, N. S., *et al.* (1998) *Acta Crystallogr. D* **54,** 905–921.
34. Collaborative Computational Project Number 4 (1994) *Acta Crystallogr. D* **50,** 760–763.
35. Navaza, J. (1994) *Acta Crystallogr. A* **50,** 157–163.
36. McRee, D. E. (1999) *J. Struct. Biol.* **125,** 156–165.
37. Edman, K., Nollert, P., Royant, A., Belrhali, H., Pebay-Peyroula, E., Hajdu, J., Neutze, R. & Landau, E. M. (1999) *Nature (London)* **401,** 822–826.
38. Kraulis, P. J. (1991) *J. Appl. Crystallogr.* **24,** 946–950.
39. Merritt, E. A. & Murphy, M. E. P. (1994) *Acta Crystallogr. D* **50,** 869–873.
40. Guex, N. & Peitsch, M. C. (1997) *Electrophoresis* **18,** 2714–2723.